Biomaterials 95 (2016) 60–73

Contents lists available at ScienceDirect

Biomaterials

journal homepage: www.elsevier.com/locate/biomaterials

Tumor priming using metronomic chemotherapy with neovasculature-targeted, nanoparticulate paclitaxel

Xin Luan [a, 1], Ying-Yun Guan [a, b, 1], Jonathan F. Lovell [c], Mei Zhao [d], Qin Lu [a], Ya-Rong Liu [a], Hai-Jun Liu [a], Yun-Ge Gao [a], Xiao Dong [a], Si-Cong Yang [a], Lin Zheng [e], Peng Sun [f], Chao Fang [a, *], Hong-Zhuan Chen [a, **]

[a] Hongqiao International Institute of Medicine, Shanghai Tongren Hospital and Department of Pharmacology, Institute of Medical Sciences, Shanghai Jiao Tong University School of Medicine (SJTU-SM), 280 South Chongqing Road, Shanghai 200025, China
[b] Department of Pharmacy, Ruijin Hospital, SJTU-SM, 197 Rui Jin Er Road, Shanghai 200025, China
[c] Department of Biomedical Engineering, University at Buffalo, State University of New York, Buffalo, NY 14260, USA
[d] Department of Pharmacy, Shanghai University of Medicine & Health Sciences, 279 Zhouzhu Road, Shanghai 201318, China
[e] Pathology Center, Shanghai First People's Hospital, SJTU-SM, 280 South Chongqing Road, Shanghai 200025, China
[f] Department of General Surgery, Shanghai Tongren Hospital, SJTU-SM, 1111 Xianxia Road, Shanghai 200336, China

ARTICLE INFO

Article history:
Received 6 February 2016
Received in revised form
6 April 2016
Accepted 9 April 2016
Available online 14 April 2016

Keywords:
Tumor priming
Nanomedicine
Metronomic chemotherapy
Tumor vascular normalization
Paclitaxel

ABSTRACT

Normalization of the tumor microenvironment is a promising approach to render conventional chemotherapy more effective. Although passively targeted drug nanocarriers have been investigated to this end, actively targeted tumor priming remains to be explored. In this work, we demonstrate an effective tumor priming strategy using metronomic application of nanoparticles actively targeted to tumor neovasculature. F56 peptide-conjugated paclitaxel-loaded nanoparticles (F56-PTX-NP) were formulated from PEGylated polylactide using an oil in water emulsion approach. Metronomic F56-PTX-NP specifically targeted tumor vascular endothelial cells (ECs), pruned vessels with strong antiangiogenic activity and induced thrombospondin-1 (TSP-1) secretion from ECs. The treatment induced tumor vasculature normalization as evidenced by significantly increased coverage of basement membrane and pericytes. The tumor microenvironment was altered with enhanced pO_2, lower interstitial fluid pressure, and enhanced vascular perfusion and doxorubicin delivery. A "normalization window" of at least 9 days was induced, which was longer than other approaches using antiangiogenic agents. Together, these results show that metronomic, actively-targeted nanomedicine can induce tumor vascular normalization and modulate the tumor microenvironment, opening a window of opportunity for effective combination chemotherapies.

1. Introduction

Tumor progression is dependent upon the interaction of cancer cells with the tumor microenvironment, which consists of multiple stromal cells (infiltrating immune cells, cancer-associated fibroblastic cells, and angiogenic vascular cells) [1], signaling molecules and extracellular matrix [2], and is characterized with abnormal vasculature, hypoxia and acidity [3]. Nanoscale drug delivery platforms that target these elements of the tumor microenvironment are of considerable interest. Previous research efforts have produced nanoconstructs that respond to the elements of the tumor microenvironment, such as pH [4], matrix metalloproteinases [5] and hypoxia [6,7]. Several pioneering reports have shown that nanoscale drug delivery systems can affect the stromal cells to induce tumor immunity and challenge the suppressive tumor microenvironment [8–13]. Priming the tumor microenvironment through vascular normalization and/or solid stress alleviation has shown promising results in the enhancement of drug delivery and anticancer efficacy [14–16]. The passive accumulation of liposomal doxorubicin in tumors has ever been demonstrated to prime tumors [17]. However, there have been few reports of the effects of actively targeted nanomedicines with respect to priming the tumor

* Corresponding author.
** Corresponding author.
E-mail addresses: fangchao100@hotmail.com (C. Fang), hongzhuan_chen@hotmail.com (H.-Z. Chen).
[1] Xin Luan and Ying-Yun Guan contributed equally to this work.

http://dx.doi.org/10.1016/j.biomaterials.2016.04.008
0142-9612/

microenvironment [18].

In the past decade, anti-angiogenic therapy has acquired considerable prominence [19]. As one anti-angiogenic strategy, metronomic chemotherapy with frequent and low dose administration of certain chemotherapeutics (with short drug-free break) has achieved encouraging progress and entered into phase III trials [20–23]. We recently presented preclinical data demonstrating the concept of metronomic chemotherapy using a targeted nano-drug delivery system (nano-DDS) [24]. Compared to the free drug, metronomic chemotherapy using nano-DDS improved tumor specific biodistribution, decreased off-target effects from the inhibition of physiological angiogenesis, and reduced the total accumulated dose, which is related to secondary side-effects [24]. Recent reports suggest that metronomic chemotherapy can induce phenotypic features of tumor vascular normalization, such as increased tumor perfusion and oxygenation [25,26].

Tumor vascular normalization has been demonstrated with antiangiogenic agents [27,28]. During the "normalization window", the typically tortuous and abnormal tumor blood vessels shift to have a more mature vessel structure and give rise to homogeneous blood flow, reduced interstitial fluid pressure (IFP) and reduced hypoxia. These alterations can facilitate synergistic antitumor activity with combination treatment using chemotherapy, radiotherapy, and immunotherapy [29]. This paradigm is the principal motivation for combining antiangiogenic agents with other therapeutic modalities. However, metronomic chemotherapy together combined with other anti-cancer modalities has been disappointing in clinical trials [30,31]. One possibility is that metronomic chemotherapy may only temporarily normalize the tumor vasculature and microenvironment, and combination therapy outside the normalization window could be a predominant factor responsible for the unsatisfying clinical observations.

In this work, we explore the efficacy of a metronomic tumor-vessel targeted nanomedicine, F56-conjugated paclitaxel-loaded nanoparticles (F56-PTX-NP). F56 is a peptide ligand with high binding affinity to the Flt-1 receptor (VEGFR-1) highly expressed on tumor vascular endothelial cells (ECs) [32,33]. Paclitaxel is a classical antiangiogenic model agent [34]. We found that metronomic F56-PTX-NP resulted in a length of at least 9-day normalization window in a subcutaneous MDA-MB-231 xenograft mouse model, and significantly enhanced the antitumor effect of concomitantly injected doxorubicin (DOX) in that period. This demonstrates that tumor-vessel targeted nanomedicine, when given in a metronomic manner, can actively modulate the pathophysiological status of tumor vasculature and normalize tumor vessels and the microenvironment (Fig. 1).

2. Materials and methods

2.1. Materials, cell culture, and animals

Aldehyde poly (ethylene glycol)-poly (lactide) (aldehyde-PEG-PLA, MW 64 kDa; aldehyde-PEG unit MW 5000, PLA unit MW 59,000) and Methoxy PEG-PLA (MW 61 kDa; Methoxy PEG unit MW 5000, PLA unit MW 56,000) block copolymers were synthesized and characterized by ring opening polymerization in our lab as previously described [35] and according to the literature [36]. Paclitaxel (PTX) was supplied by Knowshine Pharmachemicals (Shanghai, China). F56 peptide (WHSDMEWWYLLG) was synthesized by GL Biochem (Shanghai, China). Doxorubicin hydrochloride, sodium cholate, coumarin 6, and 4′,6-diamidino-2-phenylindole dihydrochloride (DAPI) were from Sigma-Aldrich (St. Louis, MO). Double distilled water was obtained from a Millipore Simplicity system (Millipore, Bedford, MA). All other chemicals were of analytical grade and used without further purification.

Primary human umbilical vein endothelial cells (HUVECs) and M200 medium with LSGS were obtained from Life Technologies (Carlsbad, CA). Cells at 3 to 5 passages were used in the experiments. Human MDA-MB-231 breast cancer cells were obtained from the American Type Culture Collection (Manassas, VA) and cultured in L-15 medium supplemented with 10% fetal bovine serum (FBS) and antibiotics (100 μg/mL of streptomycin and 100 U/mL of penicillin) at 37 °C in a humidified incubator with 5% CO_2.

Female BALB/c nude mice (~20 g) were provided by Shanghai Laboratory Animal Center (Chinese Academy of Sciences, Shanghai, China). The animal experiments designed in this study were approved by the ethical committee of Shanghai Jiao Tong University School of Medicine.

2.2. Preparation and characterization of F56-PTX-NP

F56-PTX-NP were engineered by emulsion and solvent evaporation method with a following surface functionalization. Briefly, 1.5 mg PTX was dissolved in a 1 mL solution of 30 mg blend of aldehyde-PEG-PLA and Methoxy-PEG-PLA (1:9, w/w) in dichloromethane and acetone (2:1, v/v). Next, 3 mL of 1% (w/v) sodium cholate was slowly poured into the solution and then sonicate of the mixture was at 200 W for 25 s (Scientz Biotechnology, Ningbo, China). The oil in water emulsion was further diluted in 40 mL of 0.5% (w/v) sodium cholate solution and the organic solvent was removed by rotary evaporation under reduced pressure. The resulting PTX-loaded nanoparticles (PTX-NP) were collected by centrifugation (11,000 × g, 30 min, 4 °C; Eppendorf AG 5810R, Germany) and washed twice to remove the excessive emulsifier. Then, PTX-NP was incubated with F56 at a 1:3 M ratio of aldehyde to the N-terminal amine of F56. The conjugation reaction was processed in 0.01 M PBS (pH 7.4) at room temperature for 10 h in the presence of $NaCNBH_3$ as a reducing reagent. Unconjugated F56 was removed by centrifugation (11,000 × g, 30 min, 4 °C) and F56-PTX-NP was collected. The coumarin 6-labeled nanoparticles were prepared in the same way except that in the oil phase PTX was replaced or mixed with 0.05% (w/v) coumarin 6.

The morphology of the nanoparticles was observed using transmission electron microscopy (TEM) (H-600, Hitachi, Japan) and atomic force microscopy (AFM) (Multimode Scanning Probe Microscope, Digital Instruments, USA). For TEM observation, the nanoparticle sample was negatively stained with a 2% (w/v) sodium phosphotungstate solution. For AFM detection, one drop of nanoparticle suspension was mounted on metal slabs, air-dried and scanned by the AFM with a Nanoscope III in tapping mode. The particle size and zeta potential were determined using a Zetasizer Nano ZS instrument (Malvern, Worcestershire, UK).

Encapsulation efficiency was expressed as the percentage of the drug amount found in the nanoparticles to the total amount used to prepare the nanoparticles, and drug loading was expressed as the percentage of the drug amount found in the nanoparticles. The amount of paclitaxel and coumarin 6 was determined by high performance liquid chromatography (HPLC, Shimadzu Corporation, Japan) methods. The peptide conjugation efficiency (CE%) was determined by estimating the amount of nanoparticle-associated peptide using CBQCA Protein Quantitation Kit (Life Technologies, Carlsbad, CA). The calculation formula is as follows: CE% = (amount of F56 conjugated on the nanoparticle surface/total amount of F56 added) × 100%.

The colloidal stability of nanoparticles was evaluated in phosphate buffered saline (PBS, pH 7.4, 0.01 M) with 10% FBS at 37 °C according to the literature [37], and the hydrodynamic size of the nanoparticles was examined at various incubation time for 24 h.

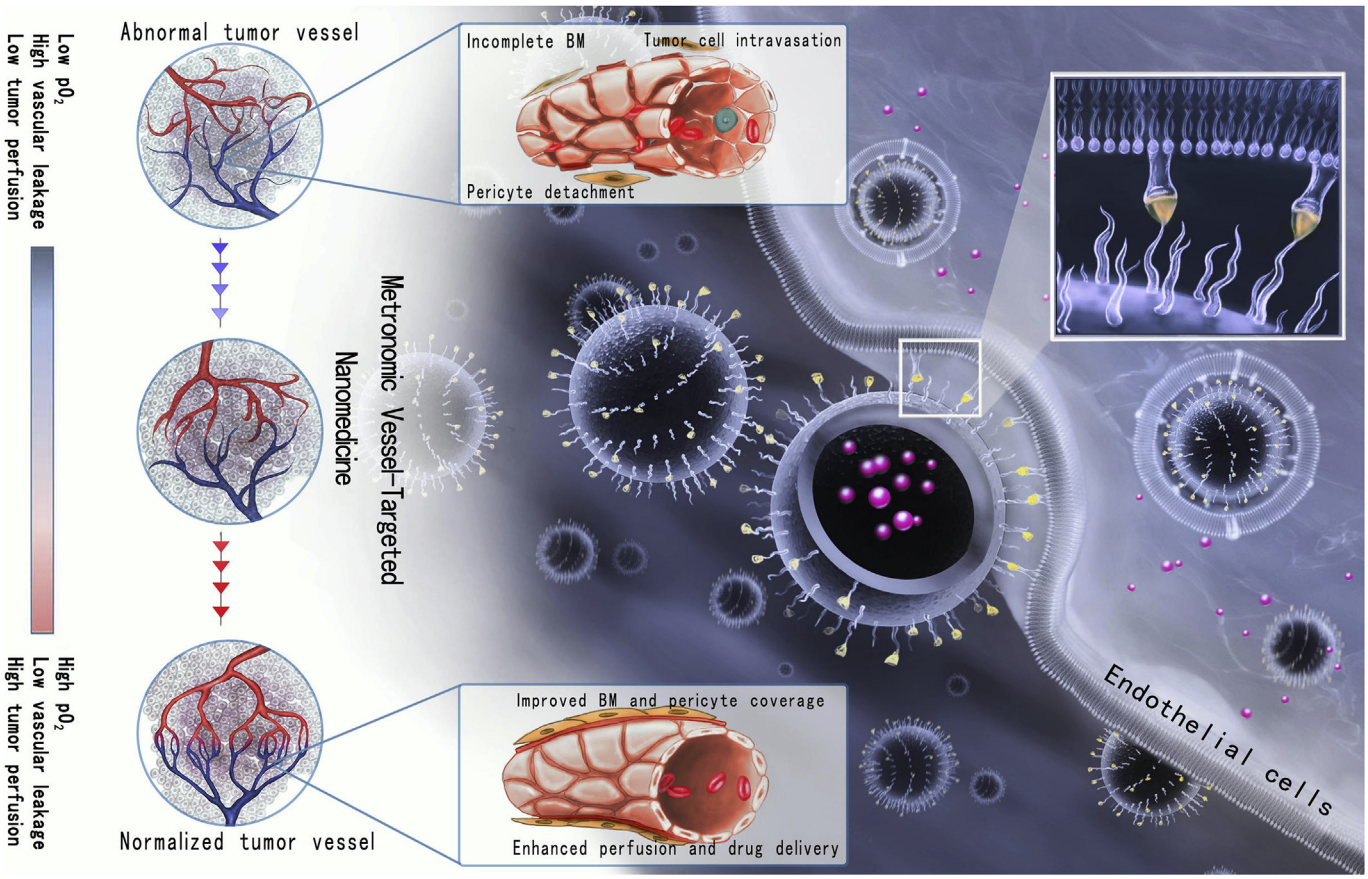

Fig. 1. Overview of tumor vascular normalization after metronomic tumor-vessel targeted nanomedicine. Metronomic F56-PTX-NP specifically target the tumor vascular ECs via multivalent peptide ligands, prune vessels through the antiangiogenic activity and induce high TSP-1 expression. The tumor vasculature is normalized through increased coverage of basement membrane (BM) and pericytes. The tumor microenvironment is consequentially transformed to the phenotypes of high pO_2, low vascular leakage, and enhanced perfusion for facilitated drug delivery.

2.3. Internalization of F56-conjugated nanoparticles in HUVECs

HUVECs is a cell model mimicking tumor vascular ECs and most widely used for the evaluation of tumor angiogenesis in vitro. For cell uptake experiments, HUVECs were cultured at a density of 5×10^3 cells/well in 96-well plates. When the cells reached about 80% confluence, the culture medium was replaced with 200 μL of coumarin 6-labeled nanoparticles (coumarin 6-labeled NP) or coumarin 6-labeled F56-conjugated nanoparticles (coumarin 6-labeled F56-NP) in medium at coumarin 6 dose of 0.2 μg/mL or 0.5 μg/mL for 0.5–12 h, respectively. After removing the nanoparticles and washing the wells three times with PBS, the cells were fixed with a 4% formaldehyde solution for 15 min, and the cell nuclei were stained with 100 ng/mL DAPI for 8 min. Then, cellular uptake was assayed by quantifying the intracellular fluorescence intensity on a Thermo Scientific ArrayScan XTI High Content Analysis Reader using a FITC filter (Ex: 490 nm, Em: 520 nm). Quantitative results were acquired based on 15 random microscope fields (containing ~1500 cells) in each well, and the tests were replicated three times.

Nanoparticle internalization was also assayed using flow cytometry. Briefly, HUVECs were cultured in 96-well plates, and were incubated with 200 μL of coumarin 6-labeled NP or F56-NP in the medium at coumarin 6 dose of 0.2 μg/mL or 0.5 μg/mL. After 2 h incubation, the cells were harvested, washed by centrifugation (1000 rpm, 10 min) for twice to remove free nanoparticles, and aliquoted up to 1×10^6 cells/100 μL PBS in FACS tubes. The cell-associated fluorescence was analyzed on Accuri C6 flow cytometer (Becton Dickinson, San Jose, CA). The cells incubated in the medium without nanoparticles were set as the negative control.

2.4. Real-time and dynamic monitoring of cell proliferation using impedance

Dynamic cell proliferation during metronomic treatment with empty F56-NP, Taxol (Bristol-Myers Squibb, Latina, Italy), and F56-PTX-NP at indicated drug concentrations were monitored in real time using a xCELLigence RTCA DP instrument (ACEA Biosciences, San Diego, CA) [38]. Briefly, 1000 HUVECs or 2000 MDA-MB-231 cells per well were seeded in E-Plate 16, and then RTCA station was placed in a humidified incubator at 37 °C with 5% CO_2. The cells were incubated in the drug-contained medium first for 8 h, and then in fresh medium for 16 h. This procedure was performed for 6 consecutive days to mimic metronomic treatment. The continuous and quantitative measurements of the cell index in each well were detected through electronic sensors. The cell index is a quantitative measure reflecting the number of the cells attached to the electrodes. The cell index is defined as $(R_n - R_b)/15$, where Rn is the cell-electrode impedance of the well when it contains cells and R_b is the background impedance of the well with the media alone.

2.5. Assay of cell viability, migration, and tube formation

HUVEC viabilities after a 6 day metronomic treatment with F56-NP, Taxol and F56-PTX-NP at the indicated drug concentrations were determined using Cell Counting Kit-8 (Dojindo Laboratories,

Kumamoto, Japan). The metronomic treatment protocol was the same to that used in the cell proliferation assay.

HUVECs migration and tube formation were assayed as previously described [35]. The HUVECs migration assay was performed after 8 h treatment in a 24-well Transwell Boyden chambers with polycarbonate filters of 8 μm pore size (Corning, Tewksbury, MA). HUVECs tube formation after 10 h treatment was evaluated using the Chemicon *In Vitro* Angiogenesis Assay Kit (Merck Millipore, Billerica, MA).

2.6. Mouse model and treatment protocol

Female BALB/c nude mice were subcutaneously inoculated with MDA-MB-231 cells (5×10^6) in the right flank. When the tumors reached ~100 mm^3 (7 days after inoculation), metronomic treatment was initiated by multiple dosing with a two-day break (day 7, 10, 13, 16, 19, 22, 25 and 28) through the caudal vein.

For the assay of the tumor vessel structure and microenvironment, four groups (21 mice in each group) were used: (1) saline (Control); (2) empty F56-NP; (3) Taxol (2.5 mg/kg); (4) F56-PTX-NP (2.5 mg/kg). At day 10, 13, 16, 19, 22, 25 and 28, three mice from each group were sacrificed, and the tumors were removed and processed for sections and immunofluorescence staining for tumor vascular ECs, pericytes, and basement membrane. The tumor oxygenation and microvessel density were evaluated at day 10, 16 and 25.

In the investigation of combination therapy, six groups (5 mice in each group) were included: (1) saline; (2) DOX (2 mg/kg) at day 16; (3) F56-PTX-NP (2.5 mg/kg); (4) F56-PTX-NP (2.5 mg/kg) + DOX (2 mg/kg) at day 10. (5) F56-PTX-NP (2.5 mg/kg) + DOX (2 mg/kg) at day 16. (6) F56-PTX-NP (2.5 mg/kg) + DOX (2 mg/kg) at day 25. The tumor volume and mice body weight were monitored throughout the study. Tumor volumes (mm^3) were calculated as $½ \times \text{length} \times \text{width}^2$. At the end of the study (day 31), the mice were sacrificed and tumors were removed, photographed, and processed for paraffin sections and pathological and immunohistochemical assay.

2.7. Immunofluorescence and immunohistochemistry

The tumor vascular ECs, pericytes and basement membrane were stained with rat anti-mouse CD31 (1: 200, BD Biosciences, Shanghai, China), rabbit anti-alpha SMA (1:200, Abcam, Hong Kong), and rabbit anti-collagen IV antibodies (1: 200, Merck Millipore, Billerica, MA), respectively. The secondary antibodies in the immunofluorescence assay were Alexa Flour 488 donkey anti-rat IgG (Life Technologies, Shanghai, China) for ECs and Alexa Flour 647 donkey anti-rabbit IgG (Life Technologies, Shanghai, China) for pericytes and basement membrane. The slides were observed with confocal fluorescence microscopy for CD31 (Ex: 495 nm, Em: BP 505–550 nm) and alpha SMA and collagen IV (Ex: 650 nm, LP Em: 668 nm). Tumor cell apoptosis and proliferation were identified using ApopTag Peroxidase *In Situ* Apoptosis Detection Kit (Merck Millipore, Billerica, MA) and mouse anti-human antibody against PCNA (Santa Cruz, CA), respectively. For the microvessel density (MVD) assay, immunohistochemistry sections stained with rat anti-mouse CD31 were photographed using a Leica DFC 320 photomicroscope and analyzed using Image-Pro Plus 6.0 software (Media Cybernetics, Bethesda, MD). Quantitative histological data were from three to five tumors per group, and five high-power fields were counted for each tumor.

2.8. 3D reconstruction of tumor vessel images

High-resolution confocal image stacks of MDA-MB-231 tumor vessels stained with anti-CD31 antibody (green) and anti-collagen IV antibody (purple) were 3D-reconstructed through isosurface rendering using Imaris software (version 7.2; Bitplane AG) [39]. This software reproduces the vessel pattern, evaluates the presence and integrity of the basement membrane, and estimates the area of tumor vascular ECs and basement membrane. The coverage ratio of basement membrane was thus calculated as the number of basement covered-ECs area to that of the total ECs area. Three fields per mouse from a total of 3 mice per group were analyzed. The 3D reconstruction images of ECs (green) and pericytes (red) were also processed using the same method.

2.9. Human TSP-1 detection in conditioned media by ELISA

HUVECs and MDA-MB-231 (1×10^3 cells/well in 96-well plate) were grown in their respective media containing F56-NP, Taxol or F56-PTX-NP at drug concentrations of 0.01, 0.1 and 1 nM, respectively, and metronomically treated with the same protocol as the cell viability assay for consecutive 6 days. The media were collected and assayed for TSP-1 using the Human Thrombospondin-1 Quantikine ELISA Kit (R&D, Minneapolis, MN) [40]. The optical density at 490 nm was determined using a microplate reader Varioskan Flash (Thermo Scientific, Waltham, MA). TSP-1 secretion from the cells treated with medium alone was set as a control.

2.10. Tumor vascular permeability

Tumor permeability was assessed by the Evans blue as previously described [41]. At day 10, 16 and 25, Evans blue (30 mg/kg) was injected intravenously to the mice and the tumors were excised 30 min later. They were dried at 60 °C for 24 h and then the dye was extracted with 1 mL formamide at 55 °C for 16 h. The concentration of the dye was determined at 620 nm.

2.11. Tumor oxygenation

At day 10, 16, and 25, 60 mg/kg pimonidazole was injected through the caudal vein to 3 mice from each group (saline, F56-NP, Taxol and F56-PTX-NP) 1 h before the tumors were harvested and processed for paraffin sections. To detect the formation of pimonidazole adducts, tumor sections were immunostained with Hypoxyprobe-1-Mab1 (Hypoxyprobe-1 Kit, Chemicon, MA) following the manufacturer's instructions. The sections were counterstained in methyl green.

Also at day 16, a fiber-optic oxygen sensor (Oxylite, Oxford Optronix, Abingdon, UK), based on the principle of oxygen quenching of luminescence, was used for tissue oxygenation pressure (pO_2) monitoring in the tumors from 6 mice in each group [42].

2.12. Tumor vascular perfusion

The Vevo 2100 micro-ultrasound imaging system (FujiFilm VisualSonics, Toronto, Canada) was used to evaluate tumor vascular perfusion [43]. Briefly, at day 16 in the metronomic treatment with F56-PTX-NP, three nude mice from each group (Saline, F56-NP, Taxol, and F56-PTX-NP) were anaesthetized with the mixture of 3.0% isofluorane and medical air mixture and placed on the warmed platform. A contrast agent (MicroMarker, VisualSonics) was prepared with a final concentration of 2×10^9 microbubbles in 1 mL saline solution, and a 50 μL bolus was delivered to the mice via tail vein catheter, and then image acquisition started. Three representative characteristic parameters (Time to Peak, Peak Enhancement, Wash in Perfusion index) describing the speed and extent of the vascular perfusion were calculated with the software

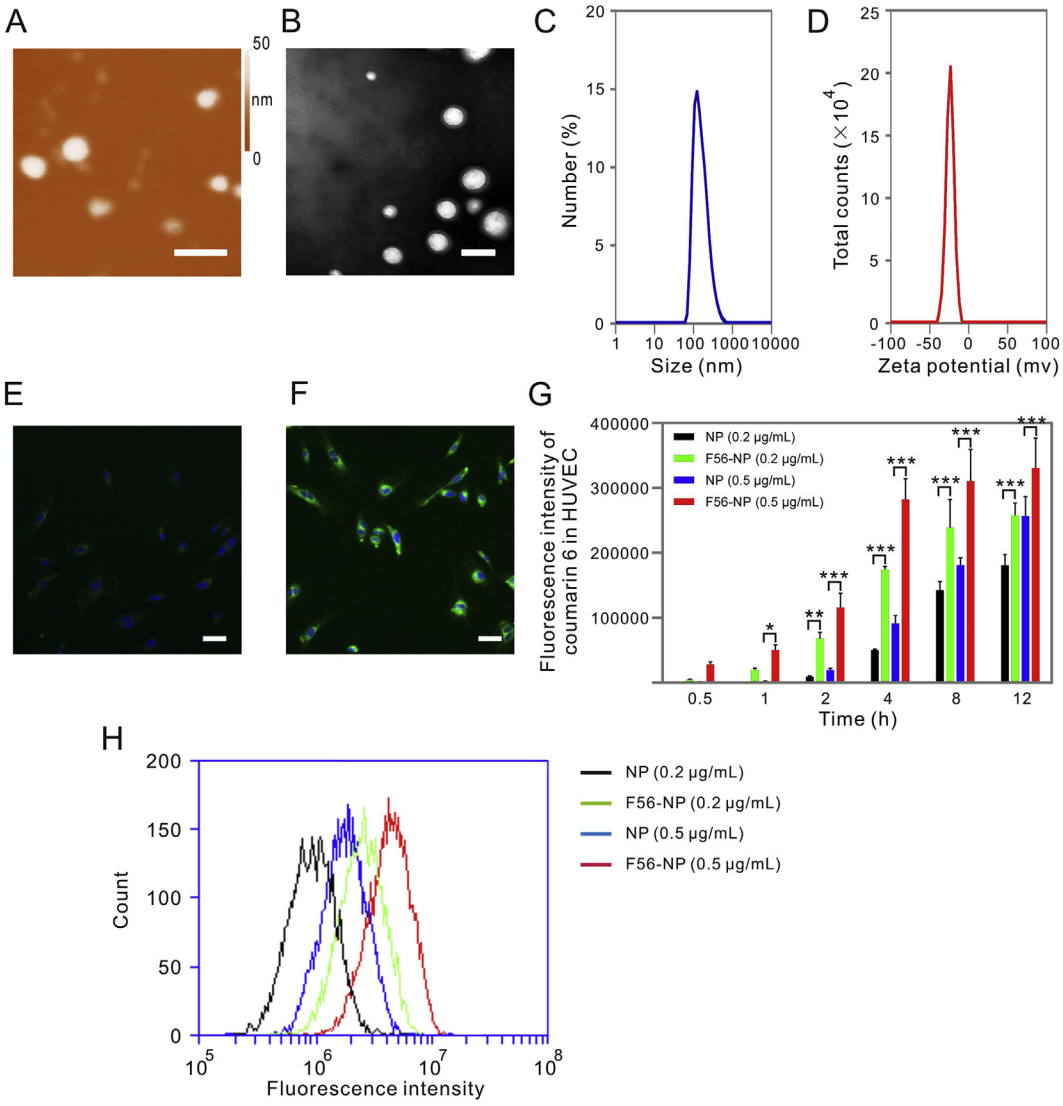

Fig. 2. Characterization and cellular uptake of F56-conjugated nanoparticles. A, AFM photograph. Bar, 200 nm. B, TEM photograph. Bar, 200 nm. C, Size determined by dynamic light scattering. D, Zeta potential. Representative HCA photographs of HUVECs after 2 h incubation with coumarin 6-labeled NP (E) and coumarin 6-labeled F56-NP (F) at coumarin 6 dose of 0.5 μg/mL. Bar, 50 μm. G, Quantitation (means ± SD, n = 5) of fluorescence intensity of coumarin 6 in HUVECs after 0.5–12 h incubation. H, HUVECs-associated fluorescence after 2 h incubation at coumarin 6 dose of 0.2 and 0.5 μg/mL was also assayed using flow cytometry.

Vevo LAB 1.7.0 (FujiFilm VisualSonics, Toronto, Canada).

2.13. Doxorubicin intratumoral distribution in combination therapy with metronomic F56-PTX-NP

DOX (5 mg/kg) was intravenously injected at day 16 to the mice treated receiving metronomic F56-PTX-NP (2.5 mg/kg) or other controls (saline, F56-NP and Taxol). At 2, 4, 6, 8 and 12 h after the injection, the tumors (3 from each group) were excised and homogenized. Proteins were precipitated by adding five volumes of acetonitrile for the DOX sample preparation. Analyses were performed, according to previous reports [44,45], on an Agilent 6410 triple quadrupole mass spectrometer (Agilent Technologies, USA) equipped with electrospray ionization (ESI) and an Agilent 1200 HPLC system (Agilent Technologies, USA). A Merck ZIC-HILIC column (2.1 mm × 100 mm, 3.5 μm) was used for analyte separation. Isocratic elution with a mobile phase consisting of acetonitrile and water (80: 20, v/v, the aqueous phase contained 0.1% formic acid) was used for the separation. Two MRM transitions, DOX (*m*/*z* 543.9–360.9, fragmentor 120 eV, collision energy 20 eV) and IS (daunorubicin, *m*/*z* 528.5–321.1, fragmentor 120 eV, collision energy 20 eV) were monitored. Data processing of MS was performed on the MassHunter software package (VersionB.04.00, Agilent Technologies, USA). The area under the curve of DOX in tumors was calculated with the WinNonlin software (Version 6.1 Pharsight, Mountain View, CA, USA) according to non-compartmental model.

2.14. Statistical analysis

Statistical analysis was conducted using GraphPad Prism 5.0 software (La Jolla, CA). Differences between groups were examined using Student's *t*-test or ANOVA with Bonferroni's multiple comparison tests. Differences were considered significant if P values were less than 0.05.

3. Results

3.1. Nanoparticle characterization and cellular uptake

AFM and TEM images showed that F56-PTX-NP were spherical

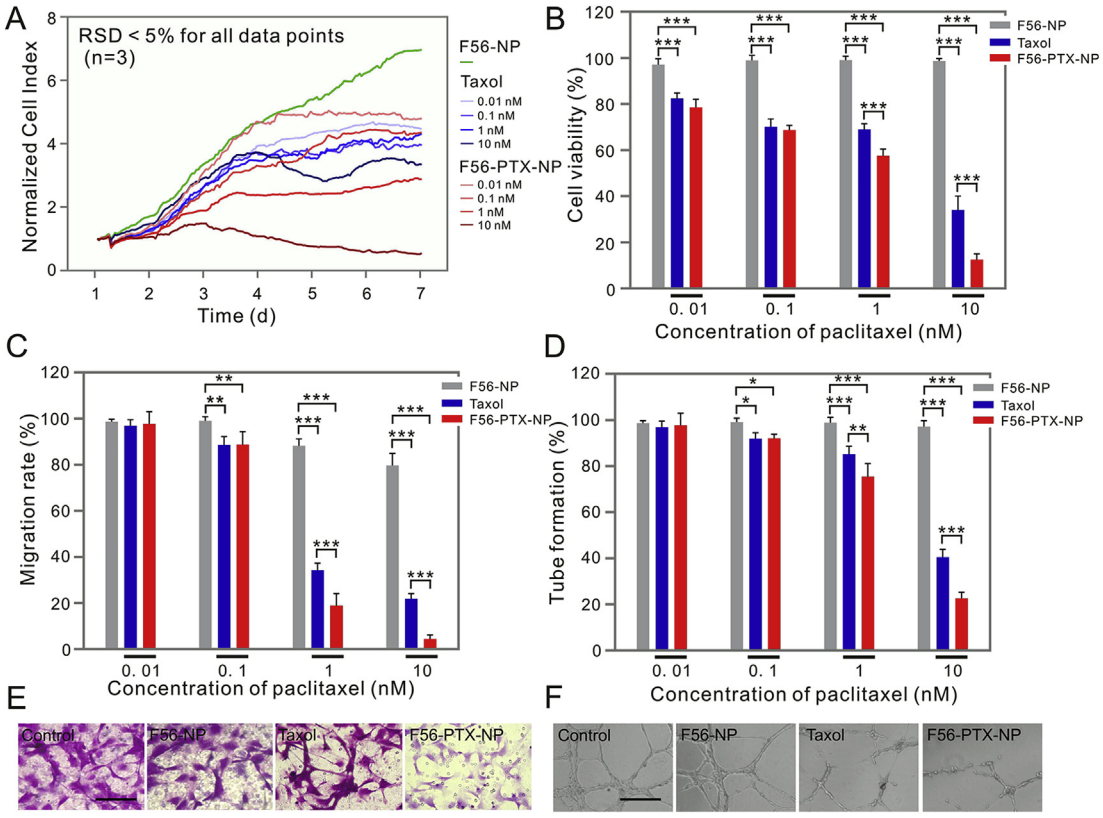

Fig. 3. F56-PTX-NP showed antiangiogenic activity of inhibiting HUVECs proliferation, viability, migration and tube formation. A, Cell proliferation was real-time and dynamic monitored using xCELLigence RTCA DP instrument in the 6-day metronomic chemotherapy. B, Cell viability at the end of the metronomic treatment was examined using CCK-8 assay. C, Cell migration after 8 h treatment was assayed using the Transwell Boyden chamber. The migrated cells were visualized by staining with crystal violet, and quantified using Image-Pro Plus 6.0 software. D, Tube formation after 10 h treatment was examined on the Matrigel pre-coated 96-well plates. The representative photographs of cell migration (E, bar 100 μm) and tube formation (F, bar 50 μm) after various treatment of 1 nM paclitaxel were shown. For empty F56-NP, the nanoparticle concentration was adjusted to be the same in all cases with nanoparticles involved. In the RTCA assay, F56-NP only at the nanoparticle concentration same to that of 10 nM F56-PTX-NP were shown. Values in B, C, and D are expressed as mean ± SD, n = 4. (For interpretation of the references to colour in this figure legend, the reader is referred to the web version of this article.)

in shape with PEG corona and no aggregation (Fig. 2A, B). The nanoparticles had hydrodynamic diameters of 164 nm (Fig. 2C), zeta potential of −21.9 mV (Fig. 2D), encapsulation efficiency of 33.7%, and drug loading of 2.9%. F56-NP had a size of 145.8 nm and a zeta potential of −20.4 mv. The nanoparticles exhibited colloidal stability in 10% FBS during 24 h incubation, and no obvious aggregation were observed (Fig. S1, Supporting information). The determined conjugation ratios of F56 were 31.8% for F56-NP, and 32% for F56-PTX-NP. Thus, it is estimated that less than 5% free aldehyde groups remained on the particle surface. F56 conjugation dramatically facilitated nanoparticle uptake in HUVECs, and this effect was dose and time-dependent, which was shown in the High Content Analysis and flow cytometry (Fig. 2E–H).

3.2. Cell growth inhibition

The xCELLigence RTCA systems, based on electrical impedance, allows real-time, rather than endpoint, and label-free measurement of cell proliferation and cytotoxicity. Moreover, the obtained cell index reflects a comprehensive characterization including cell adhesion and spreading. For HUVECs treated with 10 nM paclitaxel in Cremophor EL (Taxol), the time-dependent cell response profile (TCRP) exhibited a typically initial decline in cell index followed by a recovery rebound (Fig. 3A). Such a pattern of TCRP has been reported when cells are treated with tubulin-modulating agents such as paclitaxel [38]. In contrast, paclitaxel formulated in the F56-PTX-NP at 10 nM steadily decrease the cell index and effectively inhibited the rebound, which may be ascribed to the targeted and controlled-release properties of the nanoparticles (Fig. 3A). For MDA-MB-231 cells, a slowly increasing cell index was shown even at the highest concentration (10 nM) (data not shown), demonstrating that these tumor cells were less sensitive to paclitaxel compared to ECs.

3.3. HUVEC viability, migration and tube formation

Metronomic F56-PTX-NP led to significantly higher cytotoxicity to HUVECs compared to empty F56-NP and Taxol at drug concentrations of 1 nM and 10 nM (Fig. 3B). In contrast, nearly 80% MDA-MB-231 cells remained viable after 6-day metronomic treatment even at the highest drug concentration (10 nM) (Fig. S2, Supporting information). These results are in agreement with the observation of impedance assay and clearly demonstrated that HUVECs were more sensitive to metronomic paclitaxel, especially when the drug was formulated in the tumor-vessel targeted F56-PTX-NP. F56-NP did not decrease the viability of both cells even at the highest nanoparticle concentration corresponding to that of 10 nM F56-PTX-NP (Fig. 3B), implying that the PEG-PLA polymer and F56 peptides conjugated on the nanoparticle surface were non-toxic to the cells. Metronomic F56-PTX-NP exhibited higher activity of inhibiting HUVEC migration (Fig. 3C, E) and tube formation (Fig. 3D, F) at drug concentrations of 1 nM and 10 nM, compared to F56-NP and Taxol. These in vitro results suggested that metronomic F56-PTX-NP possesses strong antiangiogenic activity.

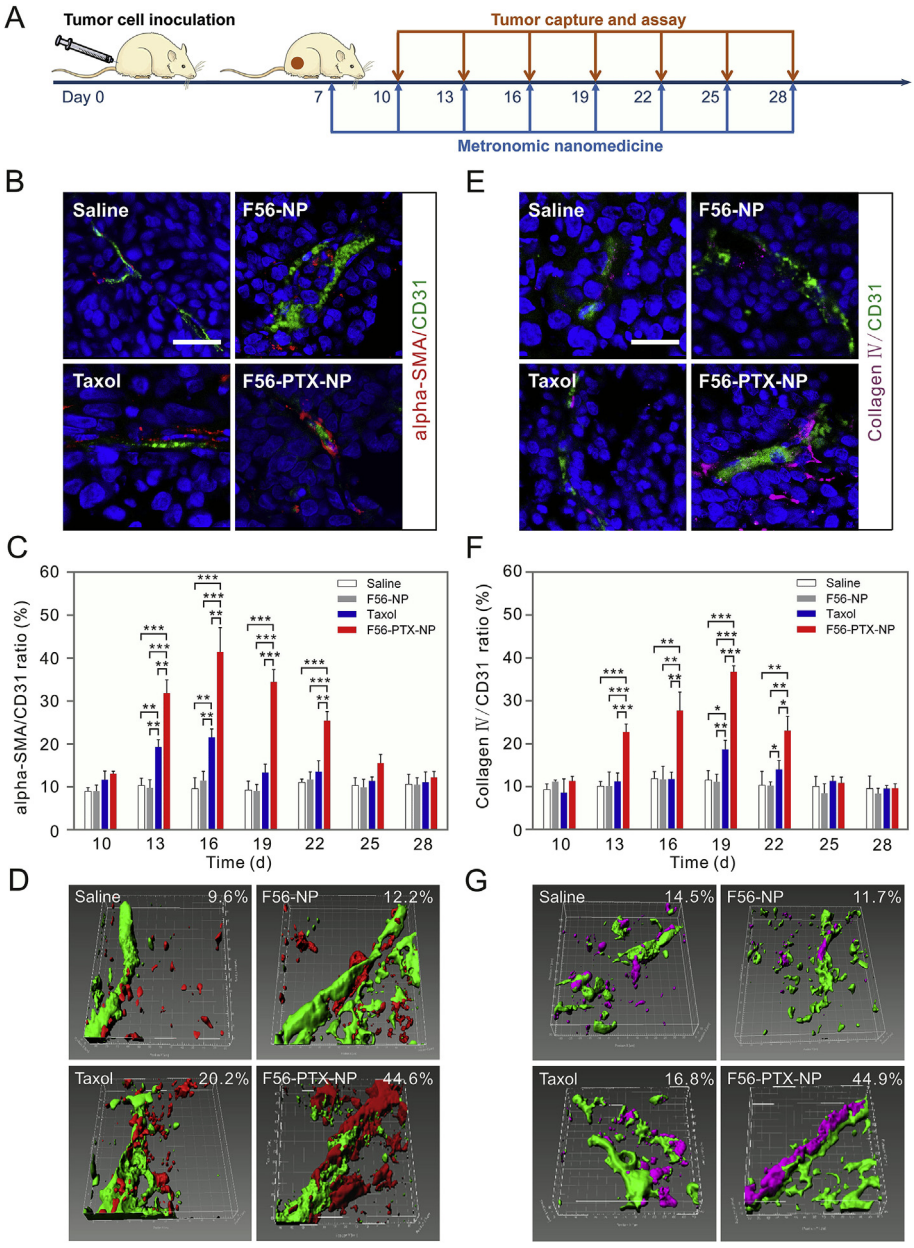

Fig. 4. Metronomic F56-PTX-NP increased the coverage of pericytes and basement membrane on the tumor vascular ECs. A, Schematic plan for the administration of F56-PTX-NP to tumor-bearing mice. At day 10, 13, 16, 19, 22, 25 and 28 in the metronomic therapy, 3 mice from each group (saline, F56-NP, Taxol and F56-PTX-NP) were sacrificed and the tumors were resected for immunofluorescence staining. The representative photographs (B and E, bar 20 μm) of immunofluorescence staining at day 16 and the quantified CD31/alpha-SMA (C) and CD31/collagen IV (F) ratio at all time points were shown. Values are expressed as mean ± SD, n = 4. The tumor vessel covered by pericytes (D) and basement membrane (G) at day 16 were 3D-reconstructed through isosurface rendering using Imaris software, and the coverage ratios are shown at the top-right corner in each image.

3.4. Pericytes and basement membrane coverage on tumor vascular ECs

Pericyte and basement membrane coverage along the vessel wall are the signatures of normalized tumor vessels [46,47]. Absent coverage and detached structures were characteristic of the tumors treated with saline, F56-NP or Taxol. In contrast, a dramatical increase in the fraction of α-SMA-positive pericytes (Fig. 4B) and collagen IV-positive basement membrane covered vessels (Fig. 4E) were observed in the tumors treated by metronomic F56-PTX-NP. The time-dependent ratio of total area of green staining (ECs) to red (pericytes) and pink (basement membrane) staining revealed an at least 9-day (from day 13 to day 22) "normalization window" in the tumors treated with F56-PTX-NP (Fig. 4C, F). Metronomic Taxol could also increase the coverage of pericytes at day 13 and 16 and basement membrane at day 19; however, such effect was much weaker than that caused by F56-PTX-NP. We chose the tumor sections of the F56-PTX-NP at day 16, when the coverage ratios reached almost the highest level, for 3D reconstruction of the vessel structure (Fig. 4D, G). The resulting images demonstrated the dramatically improved coverage of the pericytes and basement membrane on ECs in the tumors treated by metronomic F56-PTX-NP compared to other groups.

3.5. Metronomic F56-PTX-NP increases TSP-1 secretion from ECs and in tumor tissues

Enhanced TSP-1 expression is considered to be an important

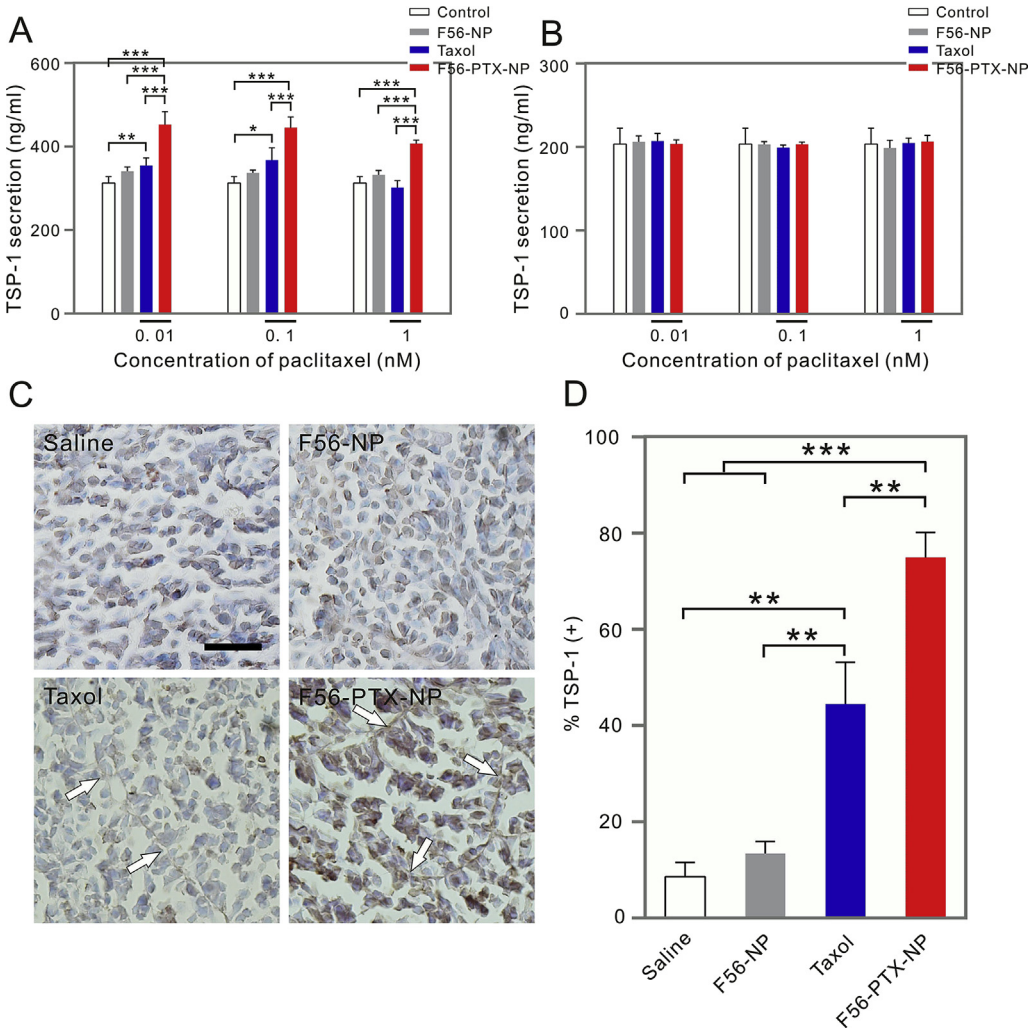

Fig. 5. Metronomic F56-PTX-NP increased TSP-1 secretion from ECs and expression in MDA-MB-231 tumor tissues. TSP-1 were specifically secreted from HUVECs (A), but not MDA-MB-231 cells (B) when exposed to 6-day metronomic F56-PTX-NP and other controls. C (Bar 50 μm) and D, TSP-1 expression was significantly increased in the tumor tissues treated with paclitaxel-contained formulations, among which F56-PTX-NP induced the highest TSP-1 expression in tumors. Noticeably, the TSP-1 expression appeared cord-like pattern (white arrows) in the tumors treated by Taxol and F56-PTX-NP. Values are expressed as mean ± SD, n = 3.

mediator of the antiangiogenic effect of metronomic chemotherapy, which has been demonstrated in a number of in vitro cell and in vivo studies involving knockout mice [40,48–50]. F56-PTX-NP significantly increased TSP-1 secretion from HUVECs up to nearly 150% compared to the control (Fig. 5A). Though the total secreted TSP-1 remained relatively stable between the different F56-PTX-NP dose treatments, the TSP-1 level when normalized to cell numbers tended to be increased, due to the significant decreased cell viability along with the increased concentration of paclitaxel (Fig. 3A, B). This phenomenon is consistent with the previous report, in which SN38 at higher concentration resulted in more TSP-1 secretion from HUVEC [40]. Taxol at 0.01 and 0.1 nM could also induce ~20% increased TSP-1 expression compared to the control (Fig. 5A). However, no pronounceable change in the TSP-1 secretion were shown from MDA-MB-231 cells subject to the same exposure (Fig. 5B). These observations were in agreement with the previous study demonstrating that TSP-1 secretion were positively modulated by metronomic SN-38 specifically in two endothelial cells (HMVEC-d and HUVECs), but remained unchanged or significantly reduced in cancer cells (HT-29 and SW620) [40].

Intriguingly, higher TSP-1 expression was observed in tumors treated by F56-PTX-NP, compared to that by F56-NP and Taxol (Fig. 5C, D). It has been reported that metronomic chemotherapy can induce strong TSP-1 secretion from perivascular tumor stromal cells [51]. Thus, it is conceivable that with long-circulating and active targeting (Fig. 2E–H) [33,35], metronomic F56-conjugated nanomedicine conferred more paclitaxel exposure than Taxol to interact with the ECs and stromal cells, and led to enhanced TSP-1 expression in tumors as shown in the immunohistochemical sections (Fig. 5C, D).

3.6. Metronomic F56-PTX-NP prunes tumor vessels, decreased vascular leakage, and improved tumor oxygenation

Dramatically decreased tumor microvessel density was observed at day 16 and 25 after metronomic treatment with F56-PTX-NP, compared to other controls (Fig. 6A, B). For Taxol, the vessel pruning effect was only observed after a longer treatment, at day 25.

The Evans blue leakage assay is a classical method to evaluate the permeability of tumor vasculature. At day 16 in the normalization window, the content of Evans blue in the tumors treated with metronomic F56-PTX-NP decreased by 41% compared to the control, 49% compared to F56-NP, and 37% compared to Taxol,

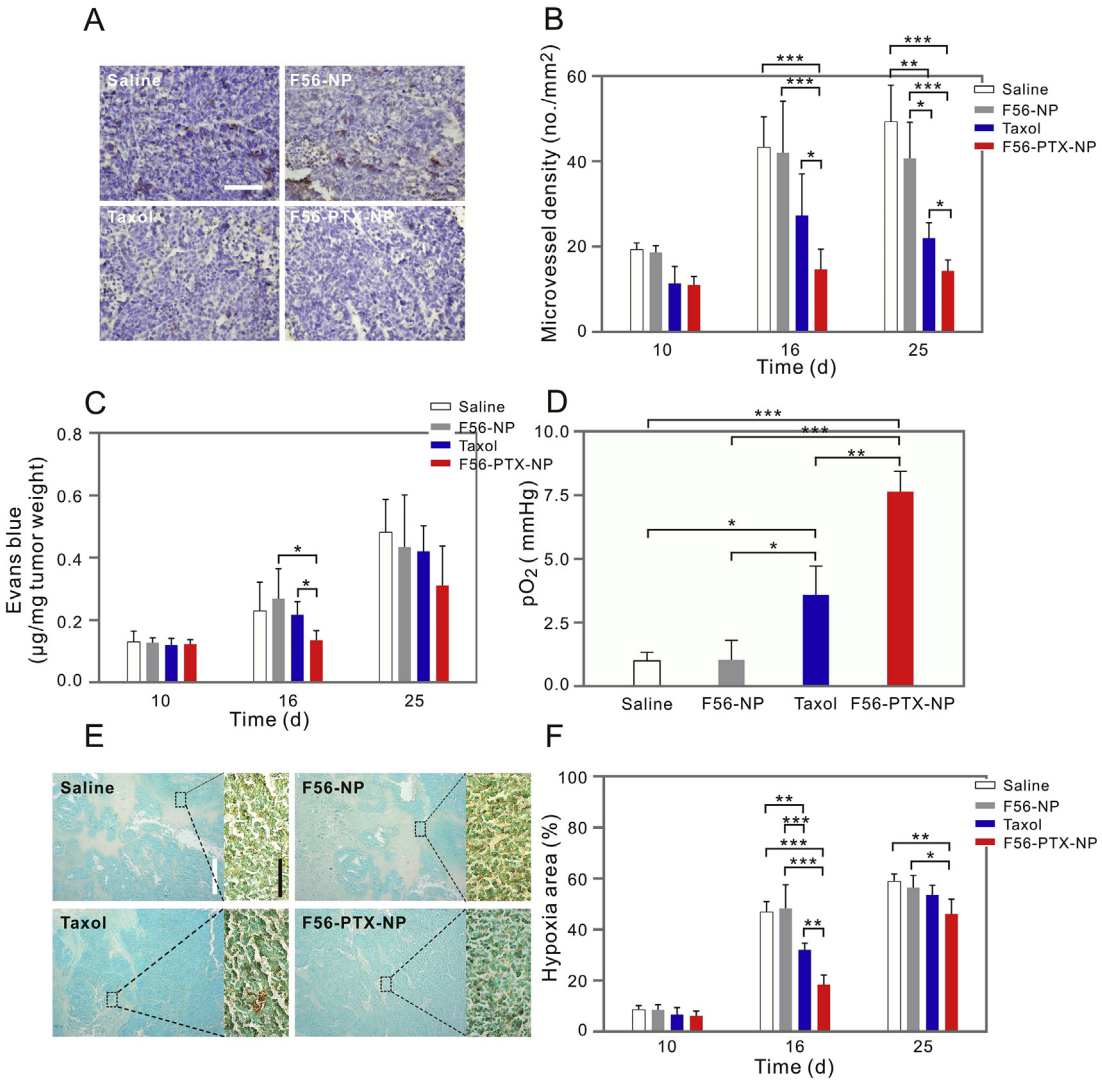

Fig. 6. Metronomic F56-PTX-NP pruned tumor vessels, decreased tumor vascular leakage, and alleviated hypoxia. The representative Immunohistochemical sections (A, Bar 75 μm) at day 16 and quantitative analysis (B) of CD31 (microvessel density, MVD) at day 10, 16, and 25 after metronomic treatment were shown. C, Tumor vascular leakage at day 10, 16 and 25 was evaluated using Evans blue as the probe. D, Tumor partial oxygen pressure (pO_2) at day 16 was examined using an Oxylite fiber-optic oxygen sensor. Representative photographs of the immunohistochemical sections stained with Hypoxyprobe-1-Mab1 at day 16 (E, Bar, 250 μm in low-power fields and 75 μm in high-power ones) and the quantified assay (F) of the tumor hypoxia area at day 10, 16, and 25 were shown. The hypoxia region was darkly stained and distributed mainly on the edge of necrosis area. Values are expressed as mean ± SD, n = 3.

respectively, indicating a pronouncedly declined vascular leakage (Fig. 6C) [52].

The oxygen level in the tumor microenvironment was evaluated with both a fiber-optic oxygen sensor and immunohistochemistry using the Hypoxyprobe-1-Mab1 antibody. Metronomic F56-PTX-NP resulted in a remarkable increase in pO_2 (Fig. 6D) and decrease in hypoxia area (Fig. 6E, F) in the MDA-MB-231 xenograft at day 16, compared to saline, F56-NP, and Taxol. Moreover, at day 25, hypoxic areas of the tumors in F56-PTX-NP group were still smaller compared to that in the groups of saline and F56-NP (Fig. 6E, F). Taxol treatment could also increase the pO_2 and shrink hypoxic areas, but the effect was much weaker than that of F56-PTX-NP.

3.7. Metronomic F56-PTX-NP improves tumor perfusion

At day 16 during the metronomic treatment, the tumors of the mice in F56-PTX-NP group exhibited higher perfusion-related ultrasound signal based on microbubble visualization using an ultrasound imaging system, indicating significantly enhanced perfusion in the tumors (Fig. 7A, B). Quantification of three representative parameters (Time to Peak, Peak Enhancement, and Wash in Perfusion index) characterizing the perfusion process showed that metronomic F56-PTX-NP was capable of increasing the perfusion speed and extent compared to other controls (Fig. 7C–E). Taxol treatment did not seem to improve tumor perfusion.

3.8. Metronomic F56-PTX-NP strengthens DOX antitumor efficacy by facilitating drug uptake in tumors during the normalization window

Since a normalization window was induced from day 13 to day 22 during metronomic F56-PTX-NP, we hypothesized that the antitumor efficacy of DOX could be enhanced if the drug were administered in this window (Fig. 8A). Metronomic F56-PTX-NP plus DOX at day 16 significantly delayed the growth of MDA-MB-231 tumors compared with other combination therapies before (day 10) or after (day 25) the normalization window, DOX only (day 16), and metronomic F56-PTX-NP only (Fig. 8B, C). There were

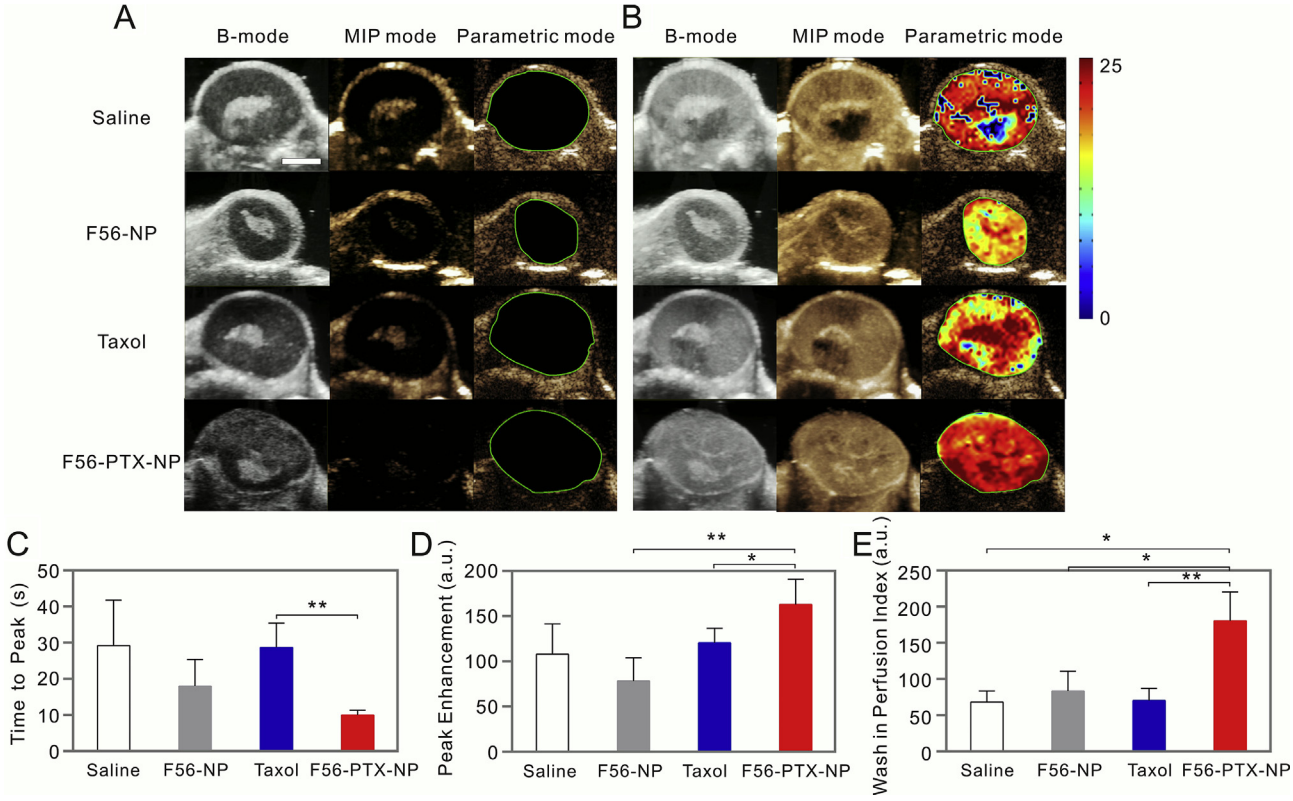

Fig. 7. Metronomic F56-PTX-NP improved tumor vascular perfusion. Tumor vascular perfusion was examined using the Vevo 2100 micro-ultrasound imaging system at day 16 during the metronomic treatment. Image acquisition was started when the contrast agent was injected to the mice. A, Tumor perfusion images at the baseline before contrast agent injection. B, Tumor images at the moment of the strongest contrast signal. Each tumor was shown in three different visualization display. B-mode (brightness mode) was acquired as original data. Maximum intensity persistence (MIP) mode showed the microvascular network distribution. Pseudo-color parametric mode displayed the intensity of perfusion kinetics. Tumors are outlined in green circles. Bar, 5 mm. Three representative parameters, Time to Peak (C), Peak Enhancement (D) and Wash in Perfusion Index (E) were statistically quantified using the Vevo LAS 1.7.0 software. Values are expressed as mean ± SD, n = 3. (For interpretation of the references to colour in this figure legend, the reader is referred to the web version of this article.)

no significant differences in body weight before and after the various treatments (Fig. 8D). Pathological and immunohistochemical analysis of tumor sections showed that DOX given during the normalization window induced by metronomic F56-PTX-NP led to significantly increased necrosis area (Fig. 8E, H), TUNEL-positive cells (Fig. 8F, I) and decreased PCNA-positive cells (Fig. 8G, J) compared with other control groups, which was consistent with the enhanced anticancer effect. The central regions of the tumors normalized by metronomic F56-PTX-NP and treated by DOX were found to be massively necrotic, and small amount of the tumor cells (<20%) at the peripheral region were proliferative and many of them (>60%) were positively stained with apoptosis indicators.

To further examine whether the enhanced curative effect was related to elevated DOX uptake in tumors, the pharmacokinetics of DOX in tumor tissues were determined using the established HPLC-MS/MS method. Metronomic F56-PTX-NP plus DOX at day 16 had the highest peak concentration and area under the curve in the tumor compared with other controls (Fig. 9A, B).

4. Discussion

Several anti-cancer nanomedicines such as Doxil and Abraxane have successfully entered the clinic, spurring interest in engineering new nano-DDS [53–56]. For targeting the tumor microenvironment, approaches have been based on “passive” response of nanoparticles due to properties such as the EPR effect, acidity, hypoxia, and elevated MMPs expression. To date limited research has made efforts of using nanomedicine to “actively” affect and modify the pathophysiology of tumor vasculature and thereby prime the tumor microenvironment. Tumor vasculature is the major component of the complex ecosystem of tumor microenvironment, and also the validated target of antiangiogenic therapy. Antiangiogenic therapy was achieved with the two emerging methods of metronomic chemotherapy and tumor-vessel targeted nanomedicine. To our knowledge, this study is the first to show that biomaterials (such as PEGylated PLA, a well biocompatible polymer), when acting as a nanocarrier for chemotherapeutics and metronomically targeted to tumor vessels, can normalize the tumor vasculature and microenvironment.

Here, we explored the effect of metronomic tumor vessel-targeted nano-DDS on the pathophysiology of tumor vasculature and microenvironment. We hypothesized there exists an underlying, but ignored, adjustment to the tumor vessel into a “normalization” status in the process of metronomic chemotherapy. We proved this postulation using F56-PTX-NP as a targeted nano-DDS model. F56-PTX-NP can specifically target and bind Flt-1 receptors highly expressed on tumor vessels in a mice model bearing MDA-MB-231 xenograft. The expression of Flt-1 in MDA-MB-231 cells was previously proved to be expressed particularly in the cytoplasm, but not on the membrane, conferring it a suitable cell model in current study [57].

The data demonstrated the targeted antiangiogenic potency of F56-PTX-NP both in vitro and in vivo. Along with the pruning effect on tumor vessels, increased coverage of pericytes and basement membrane on ECs were observed in the tumors treated with

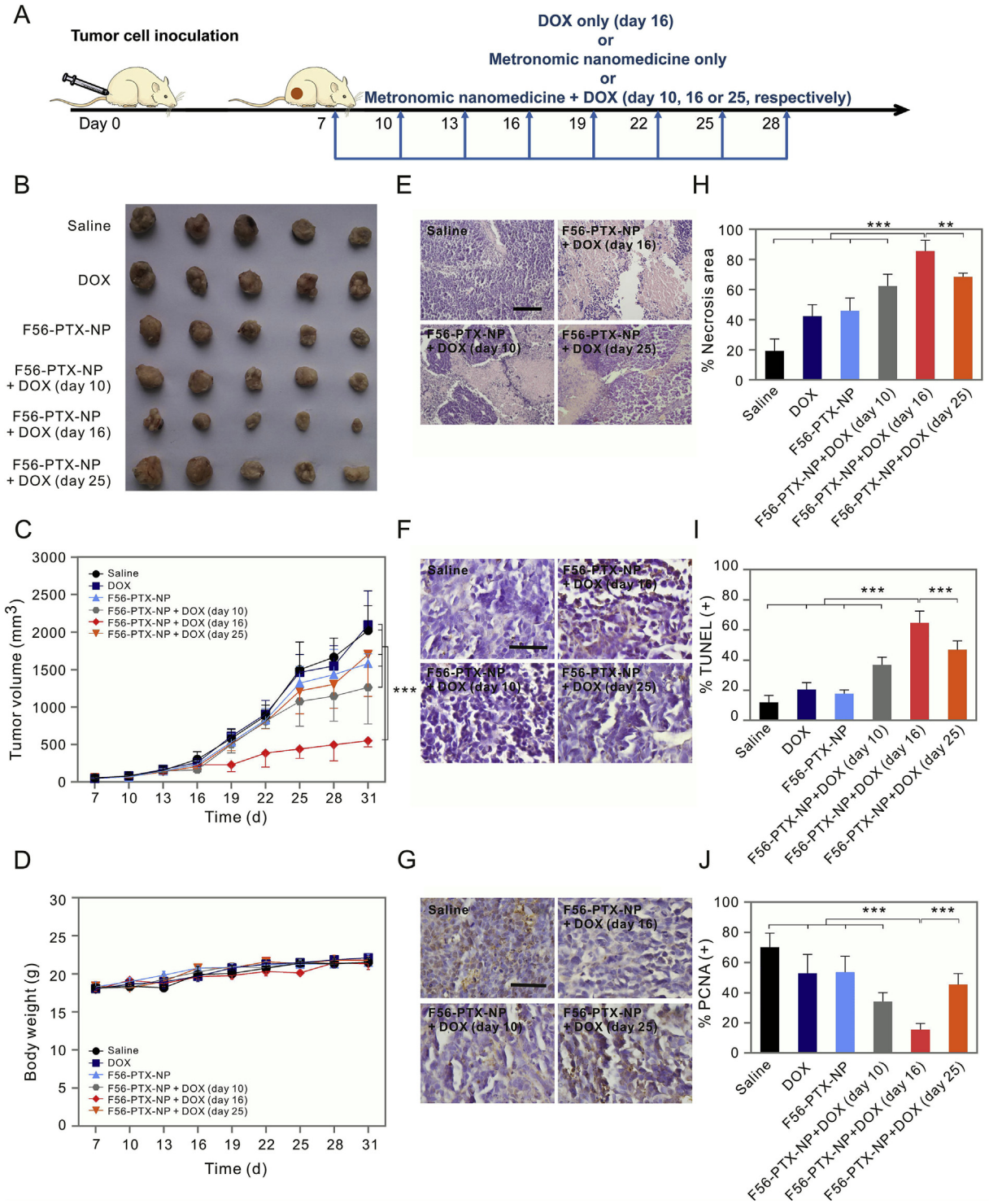

Fig. 8. Metronomic F56-PTX-NP strengthened DOX antitumor efficacy in the normalization window. (A) Schematic plan for the administration of DOX only (day 16, 2 mg/kg) or metronomic nanomedicine (2.5 mg/kg) or metronomic nanomedicine (2.5 mg/kg) plus DOX (day 10, 16 or 25, respectively, 2 mg/kg). The tumor size (B, C) and mice body weight (D) were monitored every 3 days till day 31, when mice were sacrificed and the resected tumors were photographed (B) and processed for pathological and immunohistochemical assay for the necrosis area (E, H), TUNEL (F, I) and PCNA (G, J) positive tumor cells. Bar, 75 μm in E and 50 μm in F and G. Values are expressed as mean ± SD, n = 5.

metronomic F56-PTX-NP (2.5 mg/kg with 2-day break). The time-course monitoring of the coverage ratio uncovered an at least 9-day normalization window, which lasted longer than those reported previously (<7 days) [28]. We used F56-NP as the control to exclude the contribution of the vehicle compared to F56-PTX-NP. Although non-targeted PTX-NP were not experimentally investigated in vivo in this study, the superior effect of F56-PTX-NP relative to Taxol suggests that targeted delivery of paclitaxel was better than the free, non-targeted drug in inducing vascular normalization. Moreover, our previously reported results using the same nanoparticle system and various targeting peptides demonstrated that the active targeted nanomedicines are more effective

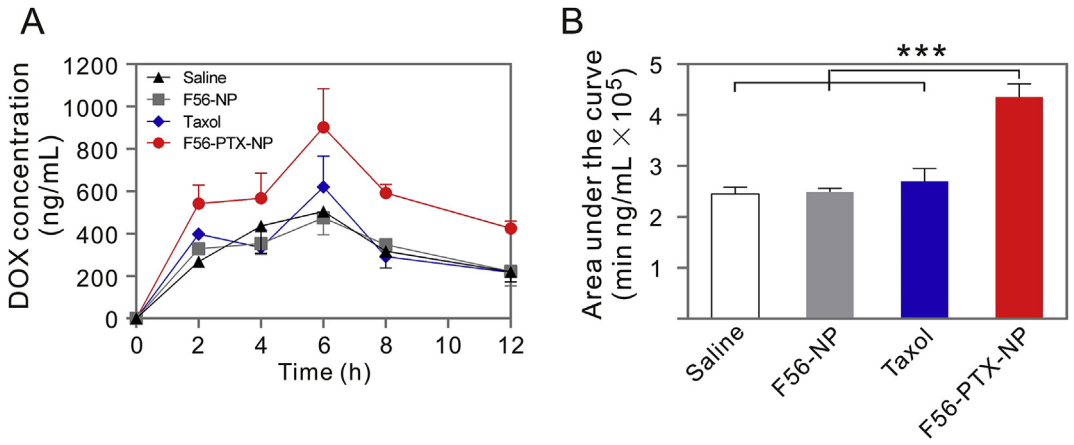

Fig. 9. Metronomic F56-PTX-NP enhanced the DOX uptake in tumor sites. DOX (5 mg/kg) was administered, at day 16 during the metronomic treatment, to the mice through the caudal vein, and the tumors of 3 mice at each time point (2, 4, 6, 8, and 12 h) after DOX injection were excised. The DOX concentration in tumor tissues were determined by LC-MS/MS. (A) DOX concentration profiles in tumors. (B) Area under the curve of DOX in tumors calculated using WinNonlin software according to non-compartmental model. Values are expressed as mean ± SD, n = 3.

than passive ones in pruning the angiogenic tumor vasculature [24,33,35], which is important for inducing tumor vascular normalization [19]. Since the abnormal tumor vasculature resulted from the overwhelming action of angiogenic stimulators, and vascular normalization is thought to be mainly achieved by restoring balance between proangiogenic and antiangiogenic signaling in the ECs, we then examined the in vitro and in vivo expression of TSP-1, a key mediator of metronomic therapy [48–50]. Metronomic treatment with F56-PTX-NP induced nearly 50% higher TSP-1 secretion specifically from HUVECs, while secretion from MDA-MB-231 cells remained unchanged. Immunohistochemical assay of TSP-1 expression after metronomic chemotherapy in vivo also demonstrated the higher TSP-1 expression in tumors treated by F56-PTX-NP. Intriguingly, we noticed TSP-1 expression appeared in a cord-like pattern in the tumors treated by Taxol and F56-PTX-NP, where the distribution of TSP-1 is well co-localized with CD31-positive ECs, confirming the specific secretion from ECs. Corresponding to the vascular normalization, Evans blue leakage decreased, pO_2 increased, and hypoxia area shrinked in the tumors of F56-PTX-NP group. Ultrasound imaging showed improved perfusion in the tumors treated by metronomic F56-PTX-NP, showing that this treatment induces the phenotype of vascular normalization. It should be realized that orthotopic breast cancer model may offer more realistic tumor microenvironment and better mimic the clinical condition. Also, tumor type and microenvironment are key factors influencing the normalization window, since tumor tends to recruit alternative pro-angiogenic pathways to escape the effects of antiangiogenic treatment and shifts to the phenotype of revascularization [58]. Thus, future studies with various orthotopic models are needed for the comparison with the findings in current study.

We performed combination therapy with metronomic F56-PTX-NP and single dose of DOX to mimic a clinical regimen in which metronomic therapy is combined with chemotherapy. Metronomic F56-PTX-NP plus DOX in the normalization window (day 16) delayed tumor growth, and the tumor size at the end of the study was 56% and 68%, respectively, smaller than that when DOX was given before (day 10) or after (day 25) the normalization window. This enhanced anticancer efficacy can be ascribed to the higher DOX concentration and distribution in the tumor. Compared to Taxol, the DOX peak concentration and area under the curve in tumors were 50% and 60% significantly increased, respectively. It is expected better efficacy can be achieved after further optimizing the regimen of both F56-PTX-NP and DOX.

To date, tumor vascular normalization remains a complex phenomenon, of which the mechanisms have not been fully elucidated. Previous studies have shown a number of new targets or methods to regulate vascular normalization [41,59–61], among which anti-angiogenic molecular-targeted agents have been discussed [28]. As metronomic therapy is also an antiangiogenic approach and it induces expression of the antiangiogenic inhibitor (TSP-1), it is possible that this strategy may also lead to vascular normalization. Such effect, though relatively weak, was shown in our study of metronomic chemotherapy with conventional Taxol. However, at the same dose and regimen, metronomic F56-PTX-NP exhibited a more robust potency to enable a more extended normalization window. This advantage can be ascribed to the favorable pharmacokinetic behavior and the ECs-targeting of F56-PTX-NP, as the modulation of vascular normalization depends much on the available dose of the antiangiogenic agents [62].

5. Conclusions

In this study, metronomic chemotherapy using tumor-vessel targeted nanomedicine led to vascular normalization, and enhanced anticancer effects from conventional chemotherapeutics (DOX) administered during the induced normalization window. The normalization window opened using the targeted nano-DDS was superior compared to conventional paclitaxel. Thus, the targeted nano-DDS appear to be well-suited for tumor priming to improve the efficacy of established chemotherapy.

Acknowledgments

This work was supported by National Basic Research Program of China (No. 2010CB529806), National Natural Science Foundation of China (No. 81272569, No. 81572998), Shanghai Municipal Science and Technology Commission (No. 14JC1491900), Innovation Program of Shanghai Municipal Education Commission (No. 13ZZ087).

Appendix A. Supplementary data

Supplementary data related to this article can be found at http://dx.doi.org/10.1016/j.biomaterials.2016.04.008.

References

[1] D. Hanahan, L.M. Coussens, Accessories to the crime: functions of cells

recruited to the tumor microenvironment, Cancer Cell 21 (2012) 309–322.
[2] P.P. Provenzano, C. Cuevas, A.E. Chang, V.K. Goel, D.D. Von Hoff, S.R. Hingorani, Enzymatic targeting of the stroma ablates physical barriers to treatment of pancreatic ductal adenocarcinoma, Cancer Cell 21 (2012) 418–429.
[3] M.R. Junttila, F.J. de Sauvage, Influence of tumour micro-environment heterogeneity on therapeutic response, Nature 501 (2013) 346–354.
[4] W. Chen, F. Meng, R. Cheng, C. Deng, J. Feijen, Z. Zhong, Facile construction of dual-bioresponsive biodegradable micelles with superior extracellular stability and activated intracellular drug release, J. Control. Release 210 (2015) 125–133.
[5] S. Ruan, X. Cao, X. Cun, G. Hu, Y. Zhou, Y. Zhang, L. Lu, Q. He, H. Gao, Matrix metalloproteinase-sensitive size-shrinkable nanoparticles for deep tumor penetration and pH triggered doxorubicin release, Biomaterials 60 (2015) 100–110.
[6] X. Wang, X. Cai, J. Hu, N. Shao, F. Wang, Q. Zhang, J. Xiao, Y. Cheng, Glutathione-triggered "off-on" release of anticancer drugs from dendrimer-encapsulated gold nanoparticles, J. Am. Chem. Soc. 135 (2013) 9805–9810.
[7] F. Perche, S. Biswas, T. Wang, L. Zhu, V.P. Torchilin, Hypoxia-targeted siRNA delivery, Angew. Chem. Int. Ed. 53 (2014) 3362–3366.
[8] J. Park, S.H. Wrzesinski, E. Stern, M. Look, J. Criscione, R. Ragheb, S.M. Jay, S.L. Demento, A. Agawu, P. Licona Limon, A.F. Ferrandino, D. Gonzalez, A. Habermann, R.A. Flavell, T.M. Fahmy, Combination delivery of TGF-beta inhibitor and IL-2 by nanoscale liposomal polymeric gels enhances tumour immunotherapy, Nat. Mater. 11 (2012) 895–905.
[9] F. Leuschner, P. Dutta, R. Gorbatov, T.I. Novobrantseva, J.S. Donahoe, G. Courties, K.M. Lee, J.I. Kim, J.F. Markmann, B. Marinelli, P. Panizzi, W.W. Lee, Y. Iwamoto, S. Milstein, H. Epstein-Barash, W. Cantley, J. Wong, V. Cortez-Retamozo, A. Newton, K. Love, P. Libby, M.J. Pittet, F.K. Swirski, V. Koteliansky, R. Langer, R. Weissleder, D.G. Anderson, M. Nahrendorf, Therapeutic siRNA silencing in inflammatory monocytes in mice, Nat. Biotechnol. 29 (2011) 1005–1010.
[10] M. Wei, N. Chen, J. Li, M. Yin, L. Liang, Y. He, H. Song, C. Fan, Q. Huang, Polyvalent immunostimulatory nanoagents with self-assembled CpG oligonucleotide-conjugated gold nanoparticles, Angew. Chem. Int. Ed. 51 (2012) 1202–1206.
[11] Z. Huang, Z. Zhang, Y. Jiang, D. Zhang, J. Chen, L. Dong, J. Zhang, Targeted delivery of oligonucleotides into tumor-associated macrophages for cancer immunotherapy, J. Control. Release 158 (2012) 286–292.
[12] P. Prasad, C.R. Gordijo, A.Z. Abbasi, A. Maeda, A. Ip, A.M. Rauth, R.S. DaCosta, X.Y. Wu, Multifunctional albumin-MnO(2) nanoparticles modulate solid tumor microenvironment by attenuating hypoxia, acidosis, vascular endothelial growth factor and enhance radiation response, ACS Nano 8 (2014) 3202–3212.
[13] Z. Xu, Y. Wang, L. Zhang, L. Huang, Nanoparticle-delivered transforming growth factor-beta siRNA enhances vaccination against advanced melanoma by modifying tumor microenvironment, ACS Nano 8 (2014) 3636–3645.
[14] I.A. Khawar, J.H. Kim, H.J. Kuh, Improving drug delivery to solid tumors: priming the tumor microenvironment, J. Control. Release 201 (2015) 78–89.
[15] J. Wang, Z. Lu, B.Z. Yeung, M.G. Wientjes, D.J. Cole, J.L. Au, Tumor priming enhances siRNA delivery and transfection in intraperitoneal tumors, J. Control. Release 178 (2014) 79–85.
[16] V.P. Chauhan, T. Stylianopoulos, J.D. Martin, Z. Popovic, O. Chen, W.S. Kamoun, M.G. Bawendi, D. Fukumura, R.K. Jain, Normalization of tumour blood vessels improves the delivery of nanomedicines in a size-dependent manner, Nat. Nanotechnol. 7 (2012) 383–388.
[17] T. Roy Chaudhuri, R.D. Arnold, J. Yang, S.G. Turowski, Y. Qu, J.A. Spernyak, R. Mazurchuk, D.E. Mager, R.M. Straubinger, Mechanisms of tumor vascular priming by a nanoparticulate doxorubicin formulation, Pharm. Res. 29 (2012) 3312–3324.
[18] S. Guo, C.M. Lin, Z. Xu, L. Miao, Y. Wang, L. Huang, Co-delivery of cisplatin and rapamycin for enhanced anticancer therapy through synergistic effects and microenvironment modulation, ACS Nano 8 (2014) 4996–5009.
[19] R.K. Jain, Antiangiogenesis strategies revisited: from starving tumors to alleviating hypoxia, Cancer Cell 26 (2014) 605–622.
[20] R.S. Kerbel, A. Grothey, Gastrointestinal cancer: rationale for metronomic chemotherapy in phase III trials, Nat. Rev. Clin. Oncol. 12 (2015) 313–314.
[21] C. Jedeszko, M. Paez-Ribes, T. Di Desidero, S. Man, C.R. Lee, P. Xu, G.A. Bjarnason, G. Bocci, R.S. Kerbel, Postsurgical adjuvant or metastatic renal cell carcinoma therapy models reveal potent antitumor activity of metronomic oral topotecan with pazopanib, Sci. Transl. Med. 7 (2015), 282ra250.
[22] R.S. Kerbel, Strategies for improving the clinical benefit of antiangiogenic drug based therapies for breast cancer, J. Mammary Gland. Biol. Neoplasia 17 (2012) 229–239.
[23] N. Andre, M. Carre, E. Pasquier, Metronomics: towards personalized chemotherapy? Nat. Rev. Clin. Oncol. 11 (2014) 413–431.
[24] D.H. Yu, F.Q. Ban, M. Zhao, Q. Lu, J.F. Lovell, F. Bai, C. Wang, Y.Y. Guan, X. Luan, Y.R. Liu, C. Fang, H.Z. Chen, The use of nanoparticulate delivery systems in metronomic chemotherapy, Biomaterials 34 (2013) 3925–3937.
[25] K.K. Cham, J.H. Baker, K.S. Takhar, J.A. Flexman, M.Q. Wong, D.A. Owen, A. Yung, P. Kozlowski, S.A. Reinsberg, E.M. Chu, C.W. Chang, A.K. Buczkowski, S.W. Chung, C.H. Scudamore, A.I. Minchinton, D.T. Yapp, S.S. Ng, Metronomic gemcitabine suppresses tumour growth, improves perfusion, and reduces hypoxia in human pancreatic ductal adenocarcinoma, Br. J. Cancer 103 (2010) 52–60.
[26] J.C. Doloff, N. Khan, J. Ma, E. Demidenko, H.M. Swartz, Y. Jounaidi, Increased tumor oxygenation and drug uptake during anti-angiogenic weekly low dose cyclophosphamide enhances the anti-tumor effect of weekly tirapazamine, Curr. Cancer Drug Targets 9 (2009) 777–788.
[27] P. Carmeliet, R.K. Jain, Principles and mechanisms of vessel normalization for cancer and other angiogenic diseases, Nat. Rev. Drug Discov. 10 (2011) 417–427.
[28] R.K. Jain, A new target for tumor therapy, N. Engl. J. Med. 360 (2009) 2669–2671.
[29] S. Goel, A.H. Wong, R.K. Jain, Vascular normalization as a therapeutic strategy for malignant and nonmalignant disease, Cold Spring Harb. Perspect. Med. 2 (2012) a006486.
[30] D.A. Reardon, A. Desjardins, K. Peters, S. Gururangan, J. Sampson, J.N. Rich, R. McLendon, J.E. Herndon 2nd, J. Marcello, S. Threatt, A.H. Friedman, J.J. Vredenburgh, H.S. Friedman, Phase II study of metronomic chemotherapy with bevacizumab for recurrent glioblastoma after progression on bevacizumab therapy, J. Neuro-Oncol. 103 (2011) 371–379.
[31] J.R. Sharp, E. Bouffet, D. Stempak, J. Gammon, D. Stephens, D.L. Johnston, D. Eisenstat, J. Hukin, Y. Samson, U. Bartels, U. Tabori, A. Huang, S. Baruchel, A multi-centre Canadian pilot study of metronomic temozolomide combined with radiotherapy for newly diagnosed paediatric brainstem glioma, Eur. J. Cancer 46 (2010) 3271–3279.
[32] F.M. Brunel, J.D. Lewis, G. Destito, N.F. Steinmetz, M. Manchester, H. Stuhlmann, P.E. Dawson, Hydrazone ligation strategy to assemble multifunctional viral nanoparticles for cell imaging and tumor targeting, Nano Lett. 10 (2010) 1093–1097.
[33] C. Wang, M. Zhao, Y.R. Liu, X. Luan, Y.Y. Guan, Q. Lu, D.H. Yu, F. Bai, H.Z. Chen, C. Fang, Suppression of colorectal cancer subcutaneous xenograft and experimental lung metastasis using nanoparticle-mediated drug delivery to tumor neovasculature, Biomaterials 35 (2014) 1215–1226.
[34] E. Pasquier, S. Honore, B. Pourroy, M.A. Jordan, M. Lehmann, C. Briand, D. Braguer, Antiangiogenic concentrations of paclitaxel induce an increase in microtubule dynamics in endothelial cells but not in cancer cells, Cancer Res. 65 (2005) 2433–2440.
[35] D.H. Yu, Q. Lu, J. Xie, C. Fang, H.Z. Chen, Peptide-conjugated biodegradable nanoparticles as a carrier to target paclitaxel to tumor neovasculature, Biomaterials 31 (2010) 2278–2292.
[36] Y. Nagasaki, T. Okada, C. Scholz, M. Iijima, M. Kato, K. Kataoka, The reactive polymeric micelle based on an aldehyde-ended poly(ethylene glycol)/poly(-lactide) block copolymer, Macromolecules 31 (1998) 1473–1479.
[37] C.F. Xu, H.B. Zhang, C.Y. Sun, Y. Liu, S. Shen, X.Z. Yang, Y.H. Zhu, J. Wang, Tumor acidity-sensitive linkage-bridged block copolymer for therapeutic siRNA delivery, Biomaterials 88 (2016) 48–59.
[38] Y.A. Abassi, B. Xi, W. Zhang, P. Ye, S.L. Kirstein, M.R. Gaylord, S.C. Feinstein, X. Wang, X. Xu, Kinetic cell-based morphological screening: prediction of mechanism of compound action and off-target effects, Chem. Biol. 16 (2009) 712–723.
[39] F. Maione, F. Molla, C. Meda, R. Latini, L. Zentilin, M. Giacca, G. Seano, G. Serini, F. Bussolino, E. Giraudo, Semaphorin 3A is an endogenous angiogenesis inhibitor that blocks tumor growth and normalizes tumor vasculature in transgenic mouse models, J. Clin. Investig. 119 (2009) 3356–3372.
[40] G. Bocci, A. Falcone, A. Fioravanti, P. Orlandi, A. Di Paolo, G. Fanelli, P. Viacava, A.G. Naccarato, R.S. Kerbel, R. Danesi, M. Del Tacca, G. Allegrini, Antiangiogenic and anticolorectal cancer effects of metronomic irinotecan chemotherapy alone and in combination with semaxinib, Br. J. Cancer 98 (2008) 1619–1629.
[41] M. Mazzone, D. Dettori, R. Leite de Oliveira, S. Loges, T. Schmidt, B. Jonckx, Y.M. Tian, A.A. Lanahan, P. Pollard, C. Ruiz de Almodovar, F. De Smet, S. Vinckier, J. Aragones, K. Debackere, A. Luttun, S. Wyns, B. Jordan, A. Pisacane, B. Gallez, M.G. Lampugnani, E. Dejana, M. Simons, P. Ratcliffe, P. Maxwell, P. Carmeliet, Heterozygous deficiency of PHD2 restores tumor oxygenation and inhibits metastasis via endothelial normalization, Cell 136 (2009) 839–851.
[42] K. Skrzypek, M. Tertil, S. Golda, M. Ciesla, K. Weglarczyk, G. Collet, A. Guichard, M. Kozakowska, J. Boczkowski, H. Was, T. Gil, J. Kuzdzal, L. Muchova, L. Vitek, A. Loboda, A. Jozkowicz, C. Kieda, J. Dulak, Interplay between heme oxygenase-1 and miR-378 affects non-small cell lung carcinoma growth, vascularization, and metastasis, Antioxid. Redox Signal. 19 (2013) 644–660.
[43] A. Eichten, A.P. Adler, B. Cooper, J. Griffith, Y. Wei, G.D. Yancopoulos, H.C. Lin, G. Thurston, Rapid decrease in tumor perfusion following VEGF blockade predicts long-term tumor growth inhibition in preclinical tumor models, Angiogenesis 16 (2013) 429–441.
[44] C. Sottani, P. Rinaldi, E. Leoni, G. Poggi, C. Teragni, A. Delmonte, C. Minoia, Simultaneous determination of cyclophosphamide, ifosfamide, doxorubicin, epirubicin and daunorubicin in human urine using high-performance liquid chromatography/electrospray ionization tandem mass spectrometry: bioanalytical method validation, Rapid Commun. Mass Spectrom. 22 (2008) 2645–2659.
[45] Z. Hao, B. Xiao, N. Weng, Impact of column temperature and mobile phase components on selectivity of hydrophilic interaction chromatography (HILIC), J. Sep. Sci. 31 (2008) 1449–1464.
[46] R.T. Tong, Y. Boucher, S.V. Kozin, F. Winkler, D.J. Hicklin, R.K. Jain, Vascular normalization by vascular endothelial growth factor receptor 2 blockade induces a pressure gradient across the vasculature and improves drug penetration in tumors, Cancer Res. 64 (2004) 3731–3736.
[47] J. Liu, S. Liao, Y. Huang, R. Samuel, T. Shi, K. Naxerova, P. Huang, W. Kamoun, R.K. Jain, D. Fukumura, L. Xu, PDGF-D improves drug delivery and efficacy via

vascular normalization, but promotes lymphatic metastasis by activating CXCR4 in breast cancer, Clin. Cancer Res. 17 (2011) 3638–3648.
[48] G. Bocci, G. Francia, S. Man, J. Lawler, R.S. Kerbel, Thrombospondin 1, a mediator of the antiangiogenic effects of low-dose metronomic chemotherapy, Proc. Natl. Acad. Sci. U. S. A. 100 (2003) 12917–12922.
[49] J. Ma, D.J. Waxman, Modulation of the antitumor activity of metronomic cyclophosphamide by the angiogenesis inhibitor axitinib, Mol. Cancer Ther. 7 (2008) 79–89.
[50] H. Iwamoto, T. Torimura, T. Nakamura, O. Hashimoto, K. Inoue, J. Kurogi, T. Niizeki, R. Kuwahara, M. Abe, H. Koga, H. Yano, R.S. Kerbel, T. Ueno, M. Sata, Metronomic S-1 chemotherapy and vandetanib: an efficacious and nontoxic treatment for hepatocellular carcinoma, Neoplasia 13 (2011) 187–197.
[51] Y. Hamano, H. Sugimoto, M.A. Soubasakos, M. Kieran, B.R. Olsen, J. Lawler, A. Sudhakar, R. Kalluri, Thrombospondin-1 associated with tumor microenvironment contributes to low-dose cyclophosphamide-mediated endothelial cell apoptosis and tumor growth suppression, Cancer Res. 64 (2004) 1570–1574.
[52] R.K. Jain, Normalizing tumor microenvironment to treat cancer: bench to bedside to biomarkers, J. Clin. Oncol. 31 (2013) 2205–2218.
[53] M.R. Kano, Nano-pathophysiology: a novel integrated approach to disease through application of nanotechnology, Adv. Drug Deliv. Rev. 74 (2014) 1.
[54] V. Torchilin, Tumor delivery of macromolecular drugs based on the EPR effect, Adv. Drug Deliv. Rev. 63 (2011) 131–135.
[55] M.J. Hawkins, P. Soon-Shiong, N. Desai, Protein nanoparticles as drug carriers in clinical medicine, Adv. Drug Deliv. Rev. 60 (2008) 876–885.
[56] D.D. Luo, K.A. Carter, J.F. Lovell, Nanomedical engineering: shaping future nanomedicines, Wiley Interdiscip. Rev. Nanomed. Nanobiotechnol. 7 (2015) 169–188.
[57] B. Mezquita, J. Mezquita, M. Pau, C. Mezquita, A novel intracellular isoform of VEGFR-1 activates Src and promotes cell invasion in MDA-MB-231 breast cancer cells, J. Cell. Biochem. 110 (2010) 732–742.
[58] S. Goel, D.G. Duda, L. Xu, L.L. Munn, Y. Boucher, D. Fukumura, R.K. Jain, Normalization of the vasculature for treatment of cancer and other diseases, Physiol. Rev. 91 (2011) 1071–1121.
[59] J. Hamzah, M. Jugold, F. Kiessling, P. Rigby, M. Manzur, H.H. Marti, T. Rabie, S. Kaden, H.J. Grone, G.J. Hammerling, B. Arnold, R. Ganss, Vascular normalization in Rgs5-deficient tumours promotes immune destruction, Nature 453 (2008) 410–414.
[60] S. Kashiwagi, K. Tsukada, L. Xu, J. Miyazaki, S.V. Kozin, J.A. Tyrrell, W.C. Sessa, L.E. Gerweck, R.K. Jain, D. Fukumura, Perivascular nitric oxide gradients normalize tumor vasculature, Nat. Med. 14 (2008) 255–257.
[61] C. Rolny, M. Mazzone, S. Tugues, D. Laoui, I. Johansson, C. Coulon, M.L. Squadrito, I. Segura, X. Li, E. Knevels, S. Costa, S. Vinckier, T. Dresselaer, P. Akerud, M. De Mol, H. Salomaki, M. Phillipson, S. Wyns, E. Larsson, I. Buysschaert, J. Botling, U. Himmelreich, J.A. Van Ginderachter, M. De Palma, M. Dewerchin, L. Claesson-Welsh, P. Carmeliet, HRG inhibits tumor growth and metastasis by inducing macrophage polarization and vessel normalization through downregulation of PlGF, Cancer Cell 19 (2011) 31–44.
[62] Y. Huang, T. Stylianopoulos, D.G. Duda, D. Fukumura, R.K. Jain, Benefits of vascular normalization are dose and time dependent-letter, Cancer Res. 73 (2013) 7144–7146.